Available online at www.sciencedirect.com

ScienceDirect

Ceramics International 40 (2014) 1439–1446

CERAMICS INTERNATIONAL

www.elsevier.com/locate/ceramint

Si_3N_4–TiN–SiC three particle phase composites for wear applications

Gurdial Blugan[a,*], Mousab Hadad[b,1], Thomas Graule[a], Jakob Kuebler[a]

[a]Empa, Swiss Federal Laboratories for Materials Science and Technology, Laboratory for High Performance Ceramics, Ueberlandstrasse 129, CH-8600 Duebendorf, Switzerland

[b]Empa, Swiss Federal Laboratories for Materials Science and Technology, Laboratory for Advanced Materials Processing, Feuerwerkstrasse 39, CH-3602 Thun, Switzerland

Received 28 May 2013; received in revised form 29 May 2013; accepted 4 July 2013
Available online 11 July 2013

Abstract

A three phase ceramic composite consisting of a Si_3N_4 matrix reinforced with TiN and SiC particles was prepared by hot pressing. The Si_3N_4–TiN–SiC composite material was investigated for microstructure and mechanical properties. Dry wear tests were carried out and the results compared with two phase Si_3N_4–TiN and Si_3N_4–SiC composites. The Si_3N_4–TiN–SiC was found to have an interesting combination of high abrasive wear resistance, low coefficient of friction and high hardness, which could lead to its use in very interesting wear applications.

Keywords: B. Composites; C. Wear resistance; D. Si_3N_4; E. Cutting tools

1. Introduction

Ceramic materials for cutting tools and high wear resistance applications in demanding environments have seen significant commercial and scientific interest in the last 25 years. Initially commercial products based on alumina (Al_2O_3), silicon nitride (Si_3N_4) and sialon were developed and these have recently been complimented by particle reinforced composite and layered materials for machining a range of cast irons, steels and other metals. Of these, Al_2O_3–titanium carbide (TiC) composite tools are commercially available, in addition Al_2O_3–TiC composite tools with titanium nitride (TiN) coatings are also available, e.g. SPK ceramic inserts from Kyocera (Japan), Ingersoll (Germany). Furthermore, Si_3N_4 based tools with TiN–Al_2O_3 and titanium carbon nitride (TiCN)–TiN coatings are available from companies including NGK/NTK (Japan) and Kyocera.

Si_3N_4 ceramics reinforced with TiN particles have led to an interesting group of ceramic composite materials. The addition of the TiN particles (nano or micron sized) can lead to two main effects. Firstly, if enough TiN is introduced then a percolating network is introduced in the electrically insulating Si_3N_4 matrix and a conductive ceramic which can be electro-discharge machined (EDM) is created, which can lead to a reduction of diamond grinding costs when preparing components and cutting tips [1,2]. The second effect is that the introduction of TiN into the Si_3N_4 matrix can lead to a ceramic with improved mechanical properties including strength, fracture toughness and Young's modulus [3]. Si_3N_4–TiN composites have also been shown to have improved wear resistance over monolithic Si_3N_4 especially during dry sliding wear tests [4–6]. This has made Si_3N_4–TiN composites of particular interest for the application of cutting tool materials for irons, steels and other metals. Si_3N_4–TiN composites can be made by different methods including the use of TiN, TiO_2 or Ti starting powders using hot pressing and spark plasma sintering for the densification processes and by SHS (self-propagating high-temperature synthesis).

An alternative reinforcing particle used for Si_3N_4 ceramics is silicon carbide (SiC). SiC has a high hardness (typically HV=22–32 GPa), therefore SiC particles can lead in particular to an increase in hardness over the base matrix, thus improving

*Corresponding author. Tel.: +41 58 765 4644; fax: +41 58 765 4150.
E-mail address: gurdial.blugan@empa.ch (G. Blugan).
[1]Present address: Nova Swiss, Vogelsangstrasse 24, CH-8307 Effretikon, Switzerland.

0272-8842/$ - see front matter © 2013 Elsevier Ltd and Techna Group S.r.l. All rights reserved.
http://dx.doi.org/10.1016/j.ceramint.2013.07.027

the wear resistance and can also lead to an increase in the thermal conductivity when incorporated into a Si_3N_4 matrix [7–9]. Si_3N_4/SiC composites have been produced by different methods including co-mixing with SiC particles [10,11]. Compared to TiN the electrical conductivity is lower for SiC. The addition of SiC particles can also lead to improvements in other properties, e.g. fracture toughness and strength. Si_3N_4/SiC composites are also of interest for cutting tool applications. Recently Si_3N_4/SiC composites had been developed for cutting tips with a microstructure specifically designed for the high speed industrial machining of wood [12,13].

There has been recent interest in multi-phase ceramic composites, with some ceramic composites being developed with up to five different particle phases [14–17]. These multi-phase ceramic composites (e.g. B_4C–SiC–Si–TiB_2, ZrB_2–SiC–B_4C, Al_2O_3–ZrB_2–ZrO_2, Al_2O_3–TiC–ZrO_2, etc.) are investigated for a range of mechanical properties and applications at different temperatures [15–18].

In the current work we produce a composite by co-mixing three different starting powders (Si_3N_4, TiN and SiC) as the main constituents. To date we have not come across such a particle reinforced composite in the literature. These composites were sintered by hot pressing using rare earth oxides as sintering additives. The microstructure, mechanical properties and wear behaviour is compared against two phase Si_3N_4/SiC and Si_3N_4/TiN composites. The goal is to see the combined effect of the high hardness particles (SiC) and the self-lubricating particles (TiN) on the wear properties of the Si_3N_4/SiC/TiN composites compared to the two phase composites, and therefore, to make a material suitable for use as a cutting tool.

2. Experimental

Starting powders consisting of α-Si_3N_4 (grade M11, H.C. Starck, Germany), α-SiC (grade UF25, H.C. Starck, Germany) and TiN (grade C, H.C. Starck, Germany) were prepared with a sintering additive system containing Al_2O_3 (CT3000 SG, Alcoa), $La(OH)_3$ (Auer Remy GmbH, Germany) and Y_2O_3 (grade C, H.C. Starck, Germany). The properties of the starting powders are listed in Table 1. Four different compositions were prepared, two Si_3N_4–TiN composites with 20 and 30 wt % TiN, one Si_3N_4–SiC composite and one Si_3N_4–TiN–SiC composite. The starting compositions of the four composites are presented in Table 2 in volume%.

Table 1
Starting properties of raw powders and the sintering additives.

Powder	Average d_{50} [μm]	Spec. surface area [m^2/g]	Density [g/cm^3]
Si_3N_4	0. 6	12.71	3.02
SiC	0.22	27.33	3.05
TiN	1.7	3.2	5.33
Al_2O_3	0.7	7.4	3.86
$La(OH)_3$	0.45	9.85	4.23
Y_2O_3	0.8	14.7	4.52

Table 2
Starting compositions of the different composites in volume%.

Composition	Si_3N_4	TiN	SiC	Al_2O_3	Y_2O_3	$La(OH)_3$
Si_3N_4–20TiN	83.5	11.8	0	1.9	2.8	0
Si_3N_4–30TiN	76.9	18.7	0	1.8	2.6	0
Si_3N_4–SiC	66.7	0	27.5	0.7	1.6	3.5
Si_3N_4–TiN–SiC	69.0	8.9	16.3	0.4	1.7	3.7

A water based slurry was prepared and the powders were wet milled for 48 h on a roller mill in a PET bottle with 3 mm Si_3N_4 balls. After 48 h the average particle size of the slurry was measured using laser light diffractometry (LS230, Beckman Coulter, Germany). PEG 20000 was added as a binder and the slurry milled for a further 30 min. The slip was then sieved through a 63 μm mesh and spray dried into granulates. Granulation was performed using a Minor Hi-Tec spray dryer (Niro S/A Denmark). The density of the powders initially and after spray drying was measured by He-pycnometry.

The granulated powder was die pressed into two different disc sizes (20 mm and 50 mm diameter with heights of 3 and 5 mm respectively). These were subsequently hot pressed in BN coated graphite dies. The smaller discs of the Si_3N_4–TiN–SiC ceramic were hot pressed between 1750 and 1820 °C in N_2 with a pressure of 30 MPa and a dwell time of 30 min. The small discs were used to determine the optimum sintering temperatures and to prepare polished specimens for SEM, XRD and hardness measurements. The hot pressing conditions for the Si_3N_4–TiN and Si_3N_4–SiC had been previously determined [13,19]. Samples for XRD, SEM and micro hardness were prepared by diamond grinding and final polishing using 1 μm diamond paste. XRD was performed with a PAN analytical XPert Pro diffractometer from Philips, SEM was carried out on a HR-SEM (Hitachi S-4800, Japan). Vickers hardness was performed using a Leitz Wetzlar mini-load tester (Germany).

From the large discs which were hot pressed at 1800 °C and with a pressure of 35 MPa, bars of $3\times4\times45$ mm were prepared for mechanical testing. The bars were diamond ground as specified in EN843-1 with 45° chamfers being ground on the edges [20]. Four point bending strength tests were carried out with a 20/40 mm load span and fracture toughness (K_{Ic}) was measured using the single edge v-notch beam (SEVNB) method [21]. Young's modulus (E) was also measured on these test bars by pulse excitation using a Grindo-Sonic Mark 5 (Lemmens, Belgium).

Dry friction wear tests were performed using a ball-on-flat specimen testing configuration (SRV from Optimol, Munich, Germany) with linear reciprocal sliding based on ASTM G133 [22]. The upper oscillating specimen was a 6 mm diameter Si_3N_4 bearing ball with a specified $R_a = 7$ nm and a Vickers (HV10) hardness of 1600 (grade Cerbec SN-101C, Coorstek, Connecticut, USA), as 100Cr6 steel bearing ball was previously found to be too soft and adherent. The ball acts on the bottom specimen (block) at a preselected oscillation frequency (10 Hz), stroke (2 mm) and normal load (10 N), the setup has been previously described [3]. At least three different samples were tested for each composition. The data evaluation in terms of the specific wear rate (Q) is calculated according to ASTM G133:

$$Q = \frac{\Delta V}{L F_N}$$

where ΔV is the volume loss of the test specimen, L is the total sliding distance (36 m) and F_N is the normal load applied to the specimen. The wear tracks on the specimens and ceramic balls were analysed with optical microscopy and SEM with EDX.

3. Results and discussion

3.1. Processing and microstructure

During the processing, it was found that it was beneficial for dispersion if the sintering additive powders (Al_2O_3, Y_2O_3 and $La(OH)_3$) were separately added first to the mill and milled with water and NH_3 for 30 min as this eliminated coagulation during the milling procedure (NH_3 was added to adjust the pH of the slip). At a second stage the main powder constituents Si_3N_4, TiN and/or SiC were added and milling was then continued for 48 h before spray drying. In the compositions with SiC, the laser particle analysis showed a bimodal distribution of the particles after milling (Fig. 1). The peak at approximately 0.25 μm corresponds to the SiC particles and the peak at approximately 2 μm corresponds to the Si_3N_4 and TiN, the d_{50} of the milled slurry was 1.4 μm.

The density of the spray dried powders measured by He-pycnometry was 3.551 g/cm^3 following a binder burnout treatment at 500 °C (compared to 3.43 g/cm^3 for the calculated theoretical density). This might indicate a slightly higher TiN content in the spray dried powder as a result of losing some finer SiC and Si_3N_4 powder as fines (ultra-fine powder) during the spray drying process.

Initial hot pressing trials with the 20 mm discs were carried out at 1750, 1770 and 1800 °C. After hot pressing the discs were surface ground and the densities measured by Archimedes' principle were 3.487, 3.494 and 3.497 respectively. The density results are between 98.2% and 98.5% of that of the density of the powder measured by the He-pycnometry. Following these sintering trials the large Si_3N_4–TiN–SiC discs were sintered at 1800 °C and resulted in an average density of 3.468 g/cm^3 (Table 3).

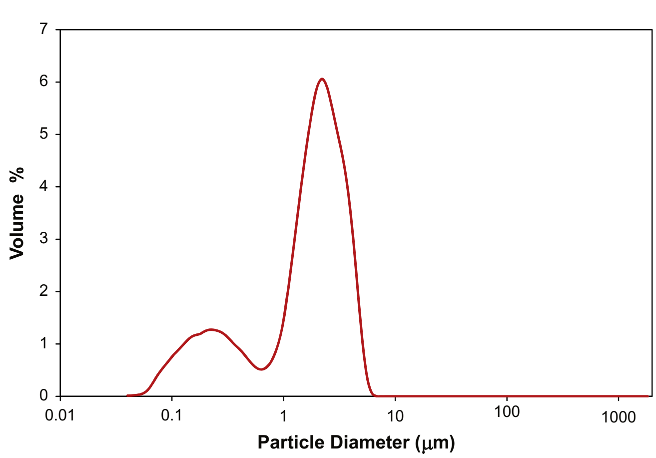

Fig. 1. Particle size analysis after milling of Si_3N_4–TiN–SiC slurry for 48 h showing the bimodal distribution of the SiC particles at approximately 0.25 μm and the Si_3N_4 and TiN particles at 1.4 μm.

The SEM examination of the plasma etched Si_3N_4–TiN–SiC shows that the TiN grains are more prevalently visible compared to that in the Si_3N_4–TiN composites (Fig. 2). The β-Si_3N_4 grains retain a fine microstructure having typical dimensions of 0.5 and 2 μm in the a and c directions respectively and appear to have the finest Si_3N_4 grain size of all the composites. What is not clearly visible in the plasma etched images is the location of the SiC grains, this will be discussed later in the fractography. The dwell time of all the materials was 30 min, with the Si_3N_4–TiN–SiC and Si_3N_4–SiC composites both having a dwell temperature of 1800 °C whilst the Si_3N_4–TiN was hot pressed at 1750 °C. Previous work has shown that the presence of SiC in Si_3N_4 hinders the densification process during sintering, requiring the need for increased sintering temperatures compared to Si_3N_4 and also the use of sintering steps where the local atmosphere is optimised [13,23]. It is clear from Fig. 2 that the β-Si_3N_4 grains in the Si_3N_4–TiN–SiC have the finest grain size whilst also achieving density greater than 98.5%, whether this is due to the effect of TiN and SiC together or in combination with the sintering additives is not clear. The XRD of the Si_3N_4–TiN–SiC confirmed the presence of the three main phases β-Si_3N_4, SiC and TiN.

3.2. Mechanical properties

The results of the mechanical tests are summarised in Table 3. An average Vickers hardness value of 1768 HV was measured for the Si_3N_4–TiN–SiC composite compared with 1810 HV for the Si_3N_4–SiC composite. Both the two Si_3N_4–TiN composites have a Vickers hardness below 1400 HV. As will be discussed later the hardness plays a significant role on the wear behaviour. Average Young's modulus measured on five test bars of the Si_3N_4–TiN–SiC was 318 GPa. This compares to 317 and 330 GPa for the Si_3N_4–20TiN and Si_3N_4–30TiN composites respectively, whilst the Si_3N_4–SiC composite has a Young's modulus of 335 GPa. The results are a little surprising in that Si_3N_4–TiN–SiC has a lower Young's modulus than both the Si_3N_4–SiC and the Si_3N_4–30TiN, as the Young's modulus which can be theoretically calculated using the rule of mixtures (Young's modulus of 320 GPa for hot pressed Si_3N_4, 400 GPa for hot pressed SiC and between 290 and 465 GPa for hot or hot isostatically pressed TiN), might be expected to be higher. This slightly low value might be due to two possible reasons, firstly the presence of small pores and secondly the relatively high volume (~5.8 vol%) of secondary additive phases. The actual effect of Young's modulus and stiffness on the wear properties of a cutting tool tip is not known. However, the tips should be stiff enough to prevent too much flexural bending when the

Table 3
Mechanical properties of sintered ceramic composites.

Composition	Av. density [g/cm^3]	Vickers hardness [HV]	K_{Ic} [MPa m$^{1/2}$]	4 Pt. bending strength [MPa]	E modulus [GPa]
Si_3N_4–20TiN	3.391	1336 (36)	4.59 (0.03)	880.4 (33.0)	317
Si_3N_4–30TiN	3.574	1396 (41)	4.69 (0.02)	780.5 (53.4)	330
Si_3N_4–SiC	3.235	1810 (52)	4.40 (0.04)	661.3 (55.6)	335
Si_3N_4–TiN–SiC	3.468	1768 (21)	4.39 (0.02)	640.5 (21.9)	318

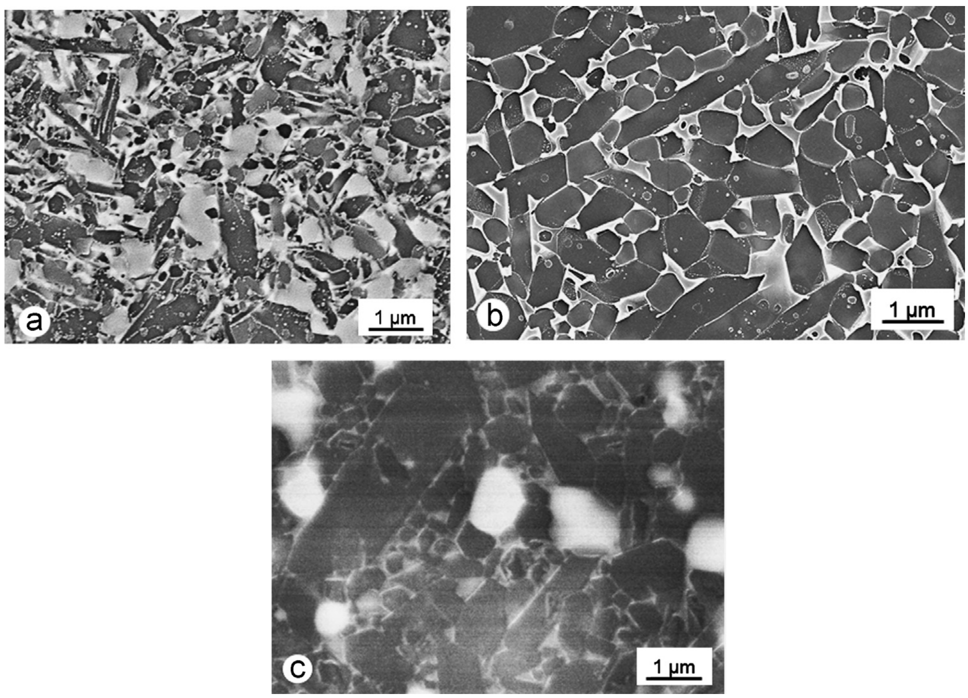

Fig. 2. SEM of plasma etched of the (a) Si_3N_4–TiN–SiC (light grains are TiN), (b) Si_3N_4–SiC and (c) Si_3N_4–20TiN composites.

cutting tip is in use due to high point loads (tip against cutting material), fixation loads (due to clamping of tip) and torsional loads (due to high speed rotation of the cutting tip or material being cut).

The average SEVNB fracture toughness of the Si_3N_4–TiN–SiC composite was confirmed as $4.39(\pm 0.02)$ MPa m$^{1/2}$ (Table 3). This compares favourably with commercially hot pressed Si_3N_4 (4.26 MPa m$^{1/2}$), although it is slightly lower than the composites reinforced with TiN and the Si_3N_4–SiC [3]. The fracture toughness plays an important role on the structural integrity of cutting tool materials. The resistance to crack propagation and also edge chipping and grain pull-out during operation is very important for ceramic cutting tools and wear applications especially at high operating speeds and loads. For example high speed wood cutting trials of Si_3N_4–SiC composites indicated that one failure mechanism is related to chipping out breaks and resulting material loss at the cutting tip edge [13,24].

The average flexural strength of Si_3N_4–TiN–SiC was confirmed as $641(\pm 22)$ MPa. The deviation in strength of six test bars is very narrow indicating that the fracture origins were all of a similar scale. However, fractography of the failure origins indicated the presence of fracture origins up to 60 μm in size. Fractography showed the failure was often caused due to porosity or agglomerates or a combination of the two together at the same location. Such a failure origin containing an agglomerate of SiC grains, fine elongated Si_3N_4 grains and an additional phase is shown in Fig. 3a. EDX analysis indicated that this phase consisted of SiO_2 containing nickel and iron. The source of this SiO_2/Fe/Ni is not yet clear since no SiO_2 raw material was added to the composition and no SiO_2 based equipment was used in the processing. SiO_2 is present on the surface of the starting α-Si_3N_4 powder but the content is less than 1 wt% and it is not normally observed in agglomerated form in the final microstructure. A stainless steel sieve was used for separating the milled slurry from the milling balls. However, if this is the source of Ni and Fe then it remains unclear why these elements are present only in combination with the SiO_2 phase.

Fractography at another fracture origin also showed another microstructural feature not observable in the polished plasma etched samples. Agglomerates of SiC grains were observed to have a clear platelet structure (see Fig. 3b). The effect of such a clustered platelet structure on mechanical and wear properties is not clear. What is clear is that the size of the defects has to be reduced when using such a composite for wear and cutting tool applications. Previously Si_3N_4/SiC composites used for wood cutting tools had tip radii of < 2 μm [12,24]. This would

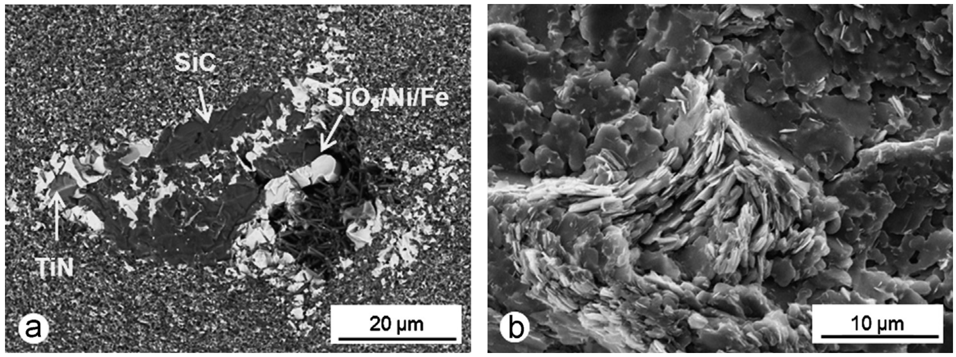

Fig. 3. (a) SEM fractography showing a fracture origin containing Si_3N_4 grains (and pores), SiC grains and a SiO_2/Ni/Fe phase agglomerated together. (b) Shows a different fracture origin where the platelet structure of SiC grains agglomerated together is clearly visible.

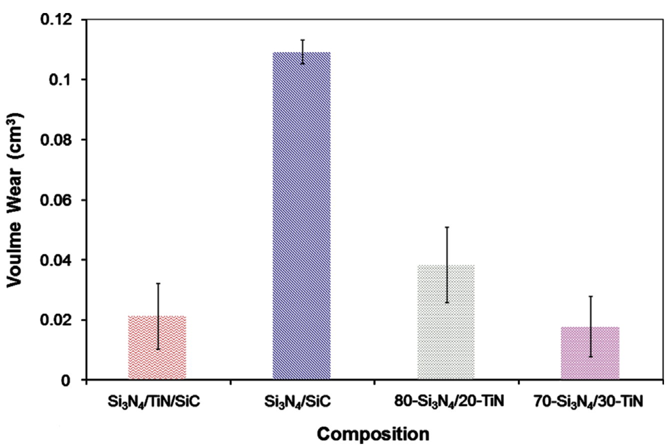

Fig. 4. Plot of the abrasive volume wear for the different compositions.

indicate that pores, agglomerates and other defects should ideally be reduced to below 5 μm for such applications.

3.3. Tribology

The dry abrasive wear results showing the wear rate are summarised in Fig. 4. The Si_3N_4–SiC composite in spite of having the highest hardness showed the highest wear rate and up to 3–4 orders of magnitude more wear than that of the other composites. The results from Fig. 4 are confirmed by the optical microscopy images of the wear tracks, an example from each composition is given in Fig. 5 that shows the biggest wear tracks were found in the Si_3N_4–SiC composite. The Si_3N_4–TiN composites show (both have a similar hardness) that the additional 10% TiN in the Si_3N_4–30TiN composite led to a significant reduction in the abrasive volume wear rate by approximately 50% compared to the Si_3N_4–20TiN.

The Si_3N_4–TiN–SiC composite shows a similar hardness as the Si_3N_4–SiC and up to four times higher wear resistance. The wear tracks of the Si_3N_4–TiN–SiC also appear to be optically the smoothest of the four compositions (Fig. 5a). This combination of properties, e.g. high hardness and high wear resistance would make it interesting for cutting tool and ball bearing applications.

The worn surfaces of the different composites were also examined by SEM to look at the wear products and to better understand the dominating wear mechanisms due to sliding in the current experimental setup. What was visible in all compositions was the smearing of Si_3N_4 wear debris on the wear track (most likely from a combination of the specimen and the ball). This is shown for the Si_3N_4–TiN–SiC composite in Fig. 6a. The wear debris appears to adhere on to the wear track, the degree of adherence is different with the different compositions. The Si_3N_4–TiN–SiC composite has the lowest amount of adhered particles on the surface. Also shown is that in general the wear appears to have a polishing effect (the smooth removal of material whilst simultaneously exposing the grains with minimum visible scratching) on large areas of the microstructure of this composite (Figs. 5a and 6b), even when that wear is against agglomerates of the SiO_2/Ni/Fe phase as shown in Fig. 6b. However, this is not the case when the ball is in interaction with agglomerates of SiC platelets (Fig. 6c), here the resistance from the harder and more abrasive particles leads to separation of the platelet grains.

The smearing appears to be with larger particles in the Si_3N_4–SiC composite (Fig. 7a). It appears that there are regions in the composite where the SiC is removed exposing Si_3N_4 grains and the intergranular phase (Fig. 7b). This debris of SiC and the Si_3N_4 from the ball leading to the production of larger and more abrasive particles in the wear debris between ball and specimen would naturally increase the wear further and is most likely the cause why this material exhibits the highest wear. The Si_3N_4–TiN composites exhibited a combination of polished areas and regions with wear debris (Fig. 7c). In the wear debris there were also large particles identified as $TiNO_x$ by EDX analysis (Fig. 7d). The presence of the polished TiN grains in the microstructure and the $TiNO_x$ phase in the wear debris are both likely to lead to the reduced wear rates that were observed, especially with increasing TiN content in the Si_3N_4–30TiN composite.

The coefficient of friction (CoF or μ) results are presented in Table 4 along with the average wear rate and the starting R_a values of the test specimens. The coefficient of friction results clearly show that increasing the TiN content in the Si_3N_4–TiN composites results in a lowering of the CoF (20% TiN $\mu = 1.57$ and 30% TiN $\mu = 1.40$), this is mainly due to the lubricious properties of TiO (at low pressure). It would be expected that the hard abrasive SiC would increase the coefficient of friction, however, surprisingly both the Si_3N_4–SiC ($\mu = 1.26$) and

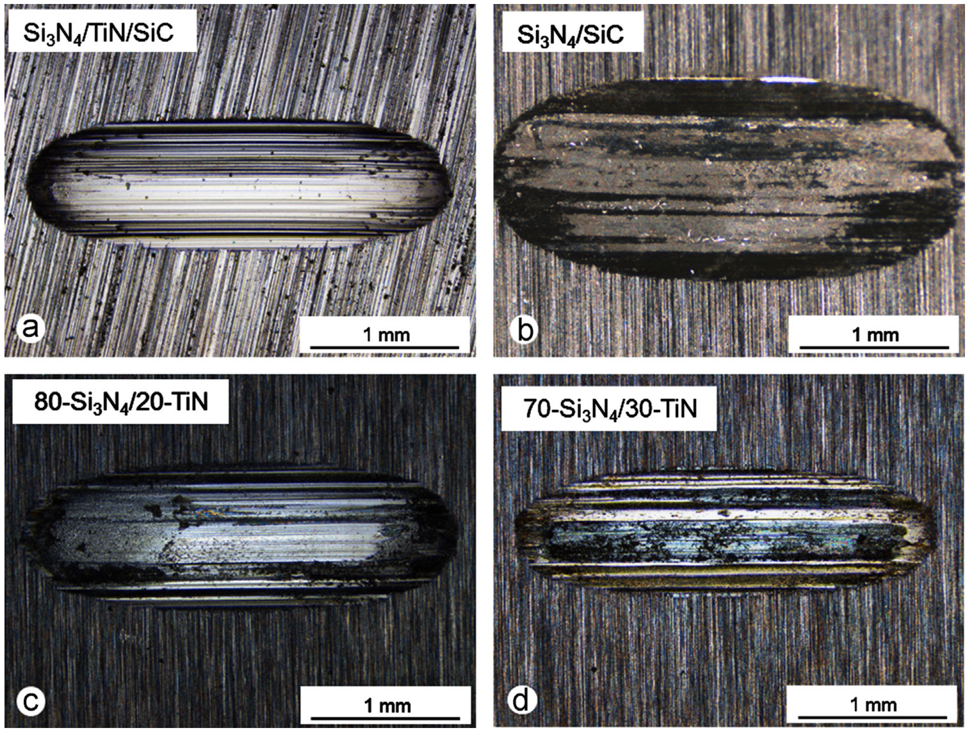

Fig. 5. The wear tracks of the different specimens (a) Si_3N_4–TiN–SiC, (b) Si_3N_4–SiC, (c) Si_3N_4–20TiN and (d) Si_3N_4–30TiN after testing for 36 m each.

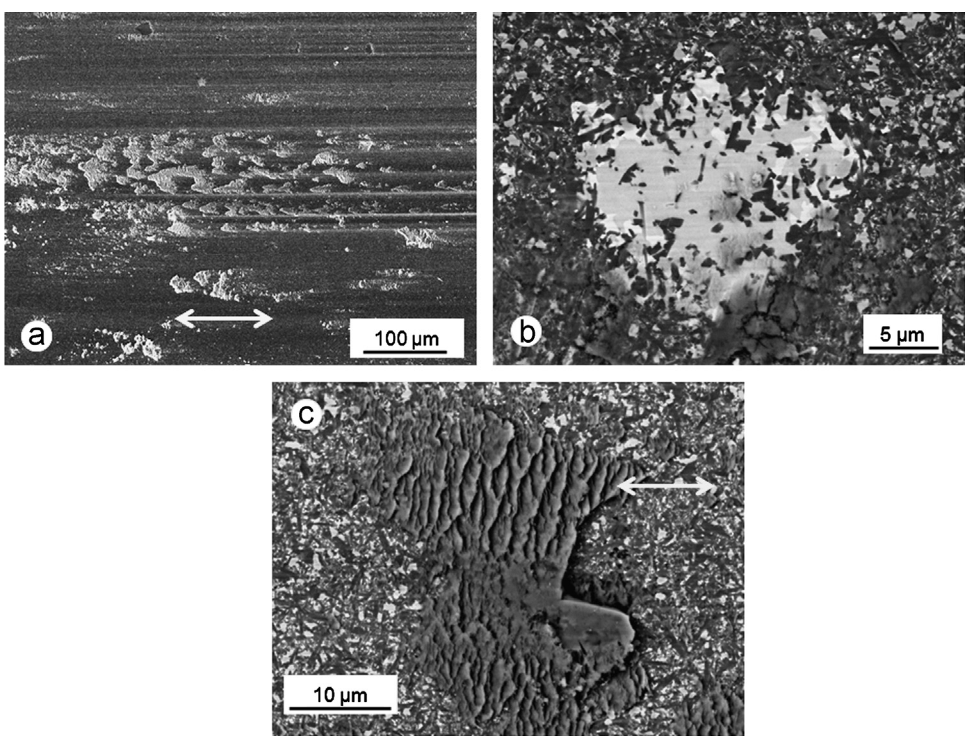

Fig. 6. Wear track of a Si_3N_4–TiN–SiC composite showing in (a) smearing of the wear track with Si_3N_4 (the white arrow indicates pin direction), (b) polishing effect of microstructure including SiO_2/Ni/Fe agglomerates and (c) the effect of agglomerates of SiC platelets.

Si_3N_4–TiN–SiC ($\mu = 1.34$) composites have an even lower value than the Si_3N_4–TiN composites. Within the scatter of the standard deviation both the latter have a very similar CoF value. It is not clear why the presence of SiC leads to a lower CoF whilst also increasing the wear rate, especially in the Si_3N_4–SiC composite. However, it may be that although the SiC is a very hard particle which plays a major role in abrasive wear it might also have a ball bearing effect to slide at the contact interface as a third body which could lead to the slight decrease in the CoF.

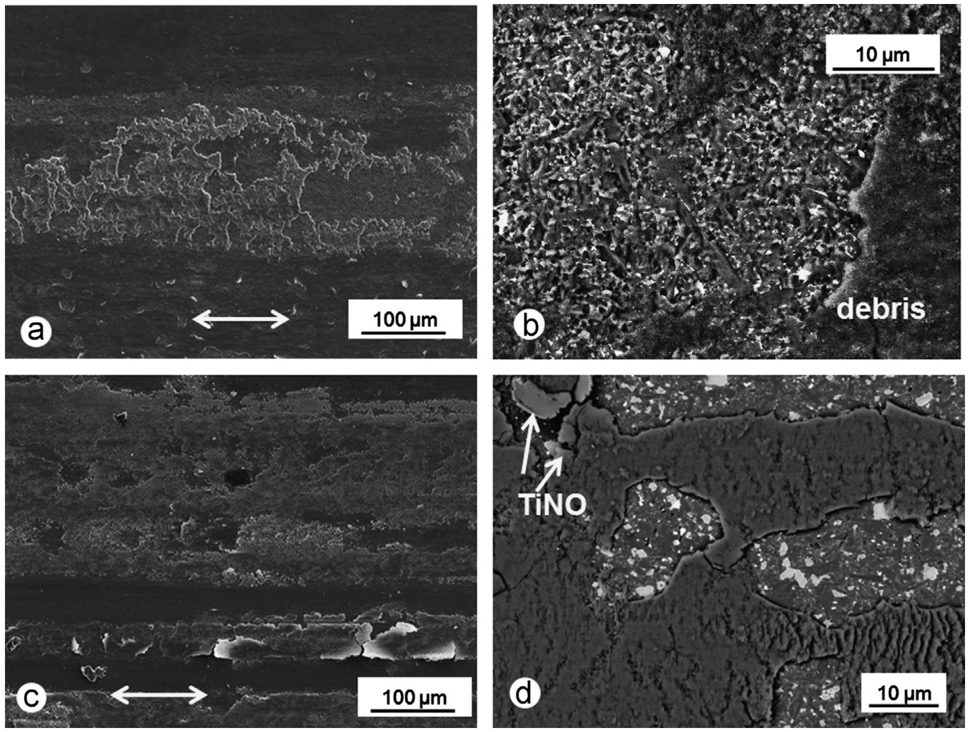

Fig. 7. Showing SEM wear tracks of (a) Si_3N_4–SiC composite, (b) the exposed Si_3N_4 grains and the SiC–Si_3N_4 wear debris on the Si_3N_4–SiC composite, (c) Si_3N_4–30TiN composite showing wear debris and polished parts of track and (d) the Si_3N_4–30TiN composite at higher magnification with polished microstructure, the Si_3N_4 debris and large TiNO particles in the wear debris.

Table 4
Summary of the tribology data for the different composites.

Composition	Starting R_a—perpendicular [µm]	Starting R_a—parallel [µm]	Coefficient of friction	Wear rate ($\times 10^{-3}$) [$mm^3\ N^{-1}\ m^{-1}$]
Si_3N_4–20TiN	0.312 (0.041)	0.121 (0.033)	1.57 (0.094)	10.66 (3.491)
Si_3N_4–30TiN	0.298 (0.039)	0.118 (0.028)	1.40 (0.071)	4.92 (2.846)
Si_3N_4–SiC	0.463 (0.081)	0.130 (0.036)	1.26 (0.080)	30.33 (3.491)
Si_3N_4–TiN–SiC	0.390 (0.053)	0.227 (0.015)	1.34 (0.092)	5.88 (1.399)

It might be interesting to determine how the CoF values change under certain application conditions, e.g. with increased temperature and/or humidity. Indeed, it is the goal to build an in-situ tribometer with a harsh conditions environmental chamber, to characterise in-situ the evolution of wear and CoF under these conditions.

The tribology tests were carried out across the direction of the grinding marks on the ceramic specimens (in the Si_3N_4–TiN–SiC composite there is a slight angle, see Fig. 5). The surface roughness R_a values are given perpendicular and parallel to the wear track direction in Table 4. The effect of the starting surface roughness on the wear rate and CoF of ceramic composites is not easy to determine, especially when there are other factors, e.g. hardness and multiple different phases, also present which contribute a higher effect.

4. Conclusions

Three phase Si_3N_4–TiN–SiC ceramic composites have been developed and produced with an interesting array of properties especially for wear related applications. These have been compared to Si_3N_4–SiC and Si_3N_4–TiN composites and found in general to have favourable properties. The Si_3N_4–TiN–SiC composite appears slightly easier to sinter than Si_3N_4–SiC, however a range of compositions would need to be prepared to confirm this effect.

The Si_3N_4–TiN–SiC composite has exhibited a low wear rate and removal combined with a polishing effect on the wear track. Only the Si_3N_4–30TiN composite has a lower wear rate. However, the Si_3N_4–TiN–SiC composite has a lower coefficient of friction and a higher hardness making it interesting for use in wear related applications including cutting tools and also ball bearings.

Of the mechanical properties the Si_3N_4–TiN–SiC appears to be very similar to the Si_3N_4–SiC in terms of strength and hardness, with K_{Ic} being slightly lower. However, the strength is lower than for the Si_3N_4–TiN composites, the later were prepared by an industrial route which included finer sieving of slurries and spray dried powders. With further process optimisation it should be possible to increase the average strength of the Si_3N_4–TiN–SiC composites by lowering the size of the defects (pores and agglomerates). The identification and removal of the source of the large SiO_2/Ni/Fe based agglomerates should also lead to an increase in the average strength.

The composition can be fine-tuned further in order to improve the wear properties and K_{Ic} further. Specifically the ratio of SiC and TiN (and content) can be altered depending on the wear characteristics and CoF required.

Acknowledgements

The authors would like to acknowledge the assistance of Empa co-workers Claudia Strehler, Roland Baechtold and Dr. Sergio De Almeida Graca for their help with processing, characterisation and tribology respectively.

References

[1] K. Liu, D. Reynaerts, B. Lauwers, Influence of the pulse shape on the EDM performance of Si_3N_4–TiN ceramic composite, CIRP Annals–Manufacturing Technology 58 (2009) 217–220.

[2] F. Bucciotti, M. Mazzocchi, A. Bellosi, Perspectives of the Si_3N_4–TiN ceramic composite as a biomaterial and manufacturing of complex-shaped implantable devices by electrical discharge machining (EDM), Journal of Applied Biomaterials and Biomechanics 8 (2010) 28–32.

[3] G. Blugan, M. Hadad, J. Janczak-Rusch, J. Kuebler, T. Graule, Fractography, mechanical properties, and microstructure of commercial silicon nitride–titanium nitride composites, Journal of the American Ceramic Society 88 (2005) 926–933.

[4] B. Zou, C. Huang, J. Song, H. Liu, H. Zhu, Cutting performance and wear mechanism of Si_3N_4-based nanocomposite ceramic cutting tool in machining of cast iron, Machining Science and Technology 15 (2011) 192–205.

[5] I. Schulz, M. Herrmann, I. Endler, I. Zalite, B. Speisser, J. Kreusser, Nano Si_3N_4 composites with improved tribological properties, Lubrication Science 21 (2009) 69–81.

[6] M. Hadad, G. Blugan, J. Kubler, E. Rosset, L. Rohr, J. Michler, Tribological behaviour of Si_3N_4 and Si_3N_4–TiN based composites and multi-layer laminates, Wear 260 (2006) 634.

[7] J.M. Carrapichano, A. Taillaire, F.J. Oliveira, R.F. Silva, Complete densification of Si_3N_4–SiC ceramic matrix composites (CMC's) by a pressureless sintering route, Materials Science Forum (2004) 225–229.

[8] P. Klimczyk, L. Jaworska, V. Urbanovich, Mechanical properties of Si_3N_4/SiC composites with various additions, Acta Metallurgica Slovaca 17 (2011) 90–98.

[9] L. Yang, J. Li, R. Wang, The research of SiC and Si_3N_4 whiskers reinforced Si_3N_4 composites to improve its wear and mechanical properties, Key Engineering Materials (2011) 1881–1886.

[10] V. Biasini, S. Guicciardi, A. Bellosi, Silicon nitride–silicon carbide composite materials, International Journal of Refractory Metals and Hard Materials 11 (1992) 213–221.

[11] D.S. Perera, M. Tokita, S. Moricca, Comparative study of fabrication of Si_3N_4/SiC composites by spark plasma sintering and hot isostatic pressing, Journal of the European Ceramic Society 18 (1998) 401–404.

[12] F. Eblagon, B. Ehrle, T. Graule, J. Kuebler, Development of silicon nitride/silicon carbide composites for wood-cutting tools, Journal of the European Ceramic Society 27 (2007) 419–428.

[13] C. Strehler, G. Blugan, B. Ehrle, B. Speisser, T. Graule, J. Kuebler, Influence of sintering and sintering additives on the mechanical and microstructural characteristics of Si_3N_4/SiC wood cutting tools, Journal of the European Ceramic Society 30 (2010) 2109–2115.

[14] J.F. Bartolomé, C.F. Gutiérrez-González, R. Torrecillas, Mechanical properties of alumina–zirconia–Nb micro–nano-hybrid composites, Composites Science and Technology 68 (2008) 1392–1398.

[15] M. Patel, J. Subrahmanyam, V.V.B. Prasad, R. Goyal, Processing and characterization of B_4C–SiC–Si–TiB_2 composites, Materials Science and Engineering: A 527 (2010) 4109–4112.

[16] Q. Dong, Q. Tang, W. Li, Al_2O_3–TiC–ZrO_2 nanocomposites fabricated by combustion synthesis followed by hot pressing, Materials Science and Engineering: A 475 (2008) 68–75.

[17] B. Li, J. Deng, Y. Li, Oxidation behavior and mechanical properties degradation of hot-pressed Al_2O_3/ZrB_2/ZrO_2 ceramic composites, International Journal of Refractory Metals and Hard Materials 27 (2009) 747–753.

[18] H. Zhang, Y. Yan, Z. Huang, X. Liu, D. Jiang, Pressureless sintering of ZrB_2–SiC ceramics: the effect of B_4C content, Scripta Materialia 60 (2009) 559–562.

[19] G. Blugan, R. Dobedoe, M. Lugovy, S. Koebel, J. Kuebler, Si_3N_4–TiN based micro-laminates with rising R-curve behaviour, Composites Part B: Engineering 37 (2006) 459.

[20] EN843-1, Advanced technical ceramics, Monolithic ceramics, Mechanical properties at room temperature, Determination of flexural strength, Advanced technical ceramics, Monolithic ceramics, Mechanical properties at room temperature, Determination of flexural strength, 1995.

[21] J. Kübler, Fracture toughness of ceramics using the SEVNB method: from a preliminary study to a standard test method, Fracture Resistance Testing of Monolithic and Composite Brittle Material, vol. 1409, ASTM STP93–106.

[22] ASTM, G133-05 Standard Test Method for Linearly Reciprocating Ball-on Flat Sliding Wear, ASTM, USA, 2010, pp. 10.

[23] M. Herrmann, C. Schuber, A. Rendtel, H. Hubner, Silicon nitride/silicon carbide nanocomposite materials: I, fabrication and mechanical properties at room temperature, Journal of the American Ceramic Society 81 (1998) 1095–1108.

[24] C. Strehler, B. Ehrle, A. Weinreich, B. Kaiser, T. Graule, C.G. Aneziris, J. Kuebler, Lifetime and wear behavior of near net shaped Si_3N_4/SiC wood cutting tools, International Journal of Applied Ceramic Technology 9 (2012) 280–290.